Development and Application of a ReaxFF Reactive Force Field for Oxidative Dehydrogenation on Vanadium Oxide Catalysts

Kimberly Chenoweth, Adri C.T. van Duin, Petter Persson,† Mu-Jeng Cheng, Jonas Oxgaard, and William A. Goddard, III*

Materials and Process Simulation Center (139-74), California Institute of Technology, Pasadena, California 91125

Received: March 11, 2008; Revised Manuscript Received: May 21, 2008

We have developed a new ReaxFF reactive force field to describe accurately reactions of hydrocarbons with vanadium oxide catalysts. The ReaxFF force field parameters have been fit to a large quantum mechanics (QM) training set containing over 700 structures and energetics related to bond dissociations, angle and dihedral distortions, and reactions between hydrocarbons and vanadium oxide clusters. In addition, the training set contains charge distributions for small vanadium oxide clusters and the stabilities of condensed-phase systems. We find that ReaxFF reproduces accurately the QM training set for structures and energetics of small clusters. Most important is that ReaxFF describes accurately the energetics for various oxidation states of the condensed phases, including V_2O_5, VO_2, and V_2O_3 in addition to metallic V (V^0). To demonstrate the capability of the ReaxFF force field for describing catalytic processes involving vanadium oxides, we performed molecular dynamics (MD) simulation for reactions of a gas of methanol exposed to the (001) surface of V_2O_5. We find that formaldehyde is the major product, in agreement with experiment. These studies find that water desorption from surface V^{III} sites is facilitated by interlayer bonding.

1. Introduction

A number of important industrial processes involve selective oxidation of unsaturated and saturated hydrocarbons by vanadium oxides. Thus, vanadyl pyrophosphate (VPO) is very active and selective for converting *n*-butane to maleic anhydride, and vanadium oxides are an important component in catalysts used to produce aldehydes, anhydrides, and acids. In particular, pure vanadium pentoxide (V_2O_5) can selectively (up to 90% at 608 K) convert methanol to formaldehyde.[1] While pure V_2O_5 works quite well for this oxidative dehydrogenation (ODH) of methanol, it is not selective enough for partial oxidation of saturated and unsaturated hydrocarbons. However, selectivity has been improved with appropriate catalyst supports, indicating that local geometric and electronic structure may influence oxidation rates and selectivity.[2]

Vanadium is also a critical component of the multimetal oxide (MMO) catalysts that selectively oxidize or ammoxidize propane, with the most promising MMO catalysts containing Mo, V, Te, Ta, and Nb.[3–6] It is generally believed that, in such MMO catalysts, the vanadium oxide species plays a critical role in activating the C−H bonds of saturated organic molecules. Due to the complexity of these systems, experimental attempts to provide detailed mechanistic insight have not been successful. Thus, it would be most valuable to use theory to establish the atomistic-level mechanistic understanding required to guide the modifications in the catalysts needed to improve activity and selectivity,

Theoretical studies to determine the mechanisms of catalytic reactions have been based on high-quality quantum mechanics (QM) because of the need to provide very accurate descriptions of the structures and energetics of the various transition states. For heterogeneous catalysts, such QM calculations are generally carried out on small nonperiodic model systems in order to allow an accurate prediction of the various reaction steps. Thus, the reaction mechanism by which $BiMoO_x$ catalysts convert propene to acrylonitrile was determined from such QM studies.[7] More pertinent to this paper is the use of QM to elucidate the mechanism for propane ODH using QM on a nonperiodic V_4O_{10} cluster.[8] This showed that the initial C−H bond activation step involves hydrogen abstraction by a vanadyl (V═O) group and led to activation energies in excellent agreement with experiment on alumina-supported V_2O_5 catalysts.[9,10] These studies also showed that the H_2O product of the ODH process would be strongly chemisorbed to the V^{III} product but that gas-phase O_2 would displace this H_2O as the first step in reoxidizing the surface, an example of the new insights that can come from QM investigations.

However, such cluster QM studies might be expected to miss many critical aspects of the heterogeneous system, with its many types of sites that might promote or poison various reaction steps. Here, periodic QM studies for a V_2O_5(001) surface[11] and for a monomeric vanadium oxide species supported on silica[12] have led to intermediates consistent with surface science experiments. QM studies have also been used to examine the methanol ODH process on V_2O_5[13] as well as on supported vanadium oxide catalysts.[14,15]

Such DFT calculations on a crystal surface become impractical for unit cells larger than 100 atoms, making them impractical for a system such as MMO, for which the periodic surface cell might require many thousands of atoms (even the bulk structure has disorder in the metal occupations). Moreover, reactions at conditions of an active catalyst (650 K or above and atmospheric pressure) may involve active intermediates and sites not accessible to QM studies at 0 K. Thus, to obtain insight into the reaction mechanisms likely to be important under experi-

* To whom correspondence should be addressed: E-mail: wag@wag.caltech.edu.
† Current address: Department of Chemical Physics, Lund University, Lund, Sweden.

10.1021/jp802134x CCC: $40.75
Published on Web 07/25/2008

mental conditions, we want to be able to follow the dynamics of the reaction processes while including the chemisorption of gas-phase substrates and oxidants onto the surface, rearrangement and reactions on the surface, and distribution of the products as a function of temperature, pressure, catalyst conditioning, and so forth. Such studies are impractical with QM.

The alternative of MD based on a classical force field (FF) has not been useful because such a FF generally cannot include the Pauli Principle effects in the QM responsible for controlling the barriers and pathways of chemical reactions. However, the recent development of the ReaxFF reactive force fields opens the possibility of an alternative to either QM or FF for simulating complex heterogeneous processes under realistic catalyst conditions.

ReaxFF has been used successfully to study the chemical transformation over a wide range of systems including combustion of hydrocarbon,[16] shock detonation of energetic materials,[17–19] thermal decomposition of polymers such as PDMS,[20] proton and oxide transport in fuel cell membranes,[21] catalytic formation of carbon nanotubes and dissociation of hydrogen over metals,[22,23] and catalytic selective oxidation of hydrocarbons over metal oxides surface.[24,25]

The aim of the ReaxFF studies reported here is to obtain a tool useful both for ODH on pure vanadium oxides and for the study of selective propane oxidation and ammoxidation on the MMO catalysts. Since changes in oxidation state between V^{III}, V^{IV}, and V^{V} play a critical role in the catalytic transformation, we have ensured that ReaxFF describes accurately the energetics for various oxidation states of the condensed phases, including V_2O_5, VO_2, V_2O_3, and the metallic state (V^0).

We report here the QM data on small clusters and bulk structures of vanadium and vanadium oxides used to derive the ReaxFF parameters, and we describe the development of the ReaxFF reactive force field. In addition, we apply ReaxFF to study the ODH of methanol to formaldehyde and the reoxidation of the active site. We find that ReaxFF accurately describes the chemical processes associated with selective oxidation of organic molecules.

2. Computational Methods

2.1. The ReaxFF Reactive Force Field Method. In ReaxFF,[26] the forces are derived from a general energy expression

$$E_{\text{total}} = E_{\text{valence}} + E_{\text{Coulomb}} + E_{\text{vdw}} \quad (1)$$

$\boldsymbol{E_{\text{valence}}}$**:** All valence terms involve a bond order dependence that goes to zero as the bonds are broken, The bond order dependence in ReaxFF uses a general relationship between bond distance and bond order whose parameters are adjusted to fit bond dissociation curves for many molecules, including systems exhibiting single, double, and triple bonds, where appropriate. The bond order is calculated directly from the instantaneous interatomic distances, which are updated continuously throughout the dynamics. Where appropriate, ReaxFF includes bond-angle-dependent and torsion-angle-dependent covalent interactions; in such cases, these terms also depend on the bond order, going to zero as any of the bonds are dissociated. For short distances, the bond order terms saturate (3 for CC and VO, 1 for CH). For highly compressed or expanded systems, this could lead to a nonphysical valence. Thus, ReaxFF includes a parameter specifying the correct valence of the atom, including terms to correct instantaneously for over- and undercoordination to achieve proper valency, allowing for smooth transitions from bonding to nonbonding interactions during reactions. Such bond length−bond order and bond order−bond energy ideas go back to Pauling[27] and were widely used by Johnston[28] and others for chemical problems. They were used in force fields for silicon materials by Tersoff[29] and in the study of hydrocarbon reactions by Brenner.[30]

$\boldsymbol{E_{\text{Coulomb}}}$**:** The electrostatic interactions between all atoms (no exclusions) are based on charges that adjust instantaneously to account for charge transfer and polarization effects. This uses a geometry-dependent charge calculation scheme[31] similar to charge equilibration with the property that Coulomb effects between bonded atoms are shielded to saturate for small distances.

$\boldsymbol{E_{\text{vdw}}}$**:** This includes all other nonbonded interactions (short-range Pauli repulsion and long-range dispersion). These terms are shielded to avoid excessive close-range nonbonded interactions

The full set of ReaxFF potential functions and force field parameters are supplied in Supporting Information. The three guiding principles used in developing ReaxFF are as follows:

(1) The energy and forces must be a continuous function of bond distances even during reactions. This is necessary so that MD simulations of reactions are continuous and well behaved. For this reason, we do not use switching functions.

(2) There can be only one force field atom type per element since during the dynamics, an atom may change its character dramatically (from sp^3 to sp^2 to sp^1 and electrophilic to nucleophilic).

(3) ReaxFF does not use predefined reactive sites or pathways allowing it to automatically handle changes in coordination associated with reactions and allowing us to discover new reaction pathways.

2.2. Fitting the ReaxFF Parameters for Vanadium Oxide Systems. The force field parameters related to H, C, and O were derived previously using the hydrocarbon oxidation training set involving nearly 1600 reactions and conditions.[16] To include reactions involving vanadium oxide systems, we also included DFT calculations for a number of additional nonperiodic and periodic systems. These were used to fit the parameters for V, H, C, and O related interactions.

Because the ReaxFF force field must describe the forces for all reasonable combinations of geometries and also a great number of unreasonable geometries, we train ReaxFF against a substantial number of QM cases, including quite a number of possible coordinations plus interaction curves describing breaking of all possible bonds. This is to ensure that the QM training set contains data relevant for each newly added combination of elements. However, we have carried out similar developments of ReaxFF force fields for quite a number of systems, all using the same or very similar functional forms. We find good transferability so that the ReaxFF for various binary combinations can be used for ternary and quaternary systems. In addition, we are gradually formulating rules based on the periodic table for developing new ReaxFF parameters. This is facilitating and making transparent parametrization for new systems.

Parameter optimization was carried using a single-parameter search optimization method[32] to minimize the sum of squares error function

$$\text{Error} = \sum_{i=1}^{n} \left[\frac{(x_{i,\text{QM}} - x_{i,\text{ReaxFF}})}{\sigma} \right]^2 \quad (2)$$

where x_{QM} is the QM value, x_{ReaxFF} is the ReaxFF calculated value, and σ is the accuracy chosen in the training set.

2.3. Quantum Mechanical Calculations. To provide the data used to parametrize ReaxFF, we performed a series of nonperiodic and periodic QM calculations. The nonperiodic QM

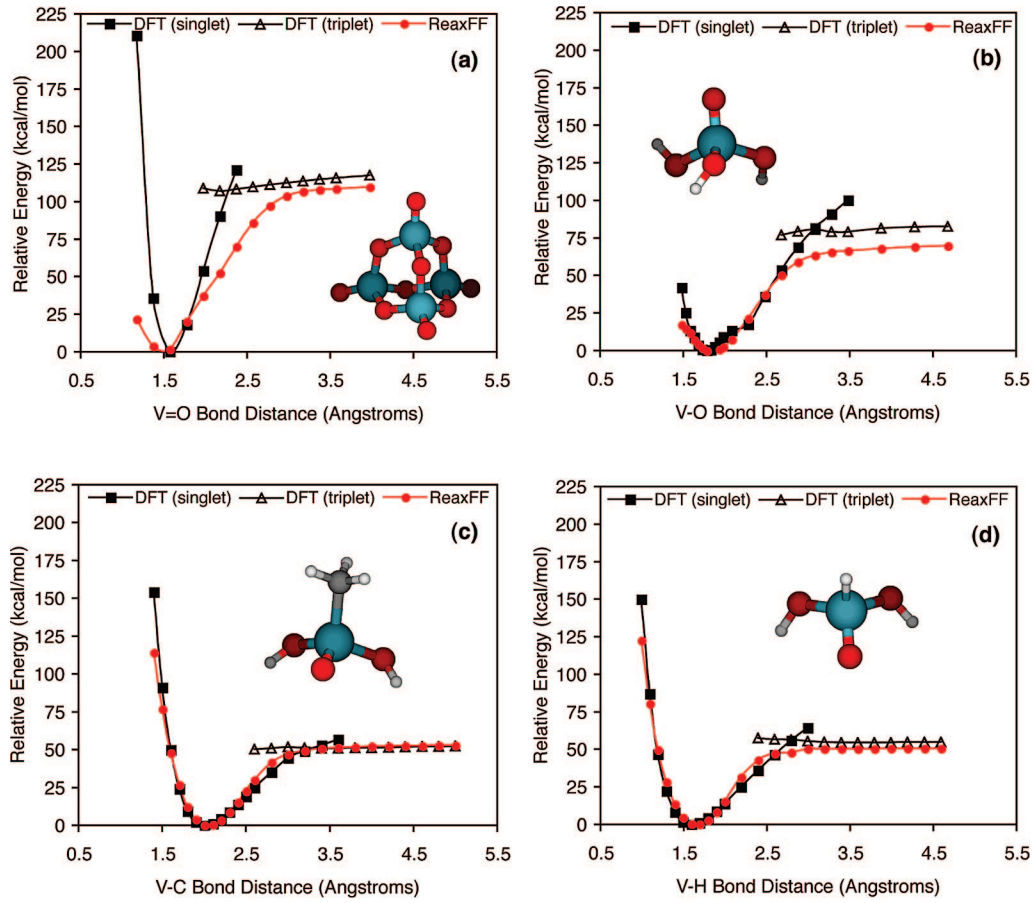

Figure 1. Comparison of ReaxFF and QM bond dissociation curves for (a) the V=O double bond in the V_4O_{10} cluster, (b) the V−O single bond in $HO-VO(OH)_2$, (c) the V−C single bond in $O=V(OH)_2CH_3$, and (d) the V−H single bond in $O=V(OH)_2H$.

calculations used the B3LYP[33] hybrid flavor of DFT as implemented in the Jaguar 7.0 program package.[34] The B3LYP flavor of DFT generally provides adequate accuracy at modest cost, reproducing thermodynamics for a wide variety of structures with a mean error of ~3 kcal/mol.[35]

For the C, O, and H atoms, all electrons were treated explicitly using the Pople 6-31G** basis set.[36] For the V atoms, we used the LACVP** Hay and Wadt[37] core valence (relativistic) effective core potential to describe the Ne inner core electrons of V, leaving 13 outer core and valence electrons to be described explicitly. The V was then described using the valence double-ζ contraction of the optimized atomic basis set.

The periodic QM calculations were performed using the SeqQuest program,[38] which uses the PBE GGA exchange-correlation functional. The Gaussian basis sets were optimized for the valence double-ζ contraction level, including polarization functions.

QM calculations were performed for all plausible spin states. For open-shell systems, QM calculations were performed using spin-unrestricted DFT (UDFT). Since ReaxFF does not have a concept of multiple spin states, it is parametrized to reproduce the energy corresponding to the lowest-energy spin state.

2.4. Molecular Dynamics Simulations. MD simulations were performed to study the oxidative dehydrogenation of methanol to form formaldehyde and subsequent regeneration of the active site. These calculations used a time step of 0.25 fs with the temperature being controlled by a Berendsen thermostat[39] with a temperature-damping constant of 0.1 ps.

To simulate the steps involved in the conversion of methanol to formaldehyde, we started with the crystal structure of V_2O_5, which has cell parameters of $a = 3.564$ Å, $b = 11.519$ Å, and $c = 4.373$ Å. We then built a 6×2 supercell in the a and b directions and used a finite slab with three layers in the c direction, leading to a (001) surface. This slab, containing 504 atoms, was exposed on both surfaces to a gas phase containing 30 methanol molecules in a volume of 8211 Å^3, which would correspond to a methanol pressure of 0.16 GPa at 2000 K. First, we optimized the CH_3OH/V_2O_5 system to minimize the energy.

Subsequent simulations of the reaction with methanol were carried out for 250 ps using a dual-temperature thermostat keeping the V and O atoms associated with the vanadium oxide slab at 650 K. while the C, O, and H atoms associated with the methanol molecules were kept at 2000 K. This temperature regime was maintained throughout the simulation and did not change when reactions occurred.

To follow the reaction events, molecular analysis of the simulations was performed using a bond order cutoff of 0.2 to allow detection of short-lived intermediates.

3. Parameterization of ReaxFF Force Field

We performed QM calculations on a wide range of systems, building a comprehensive training set selected to cover the physical and chemical properties related to the vanadium oxide and hydrocarbon system. The training set includes systems with both stable and unstable metal oxidation states and metal oxide phases with both low and high energies. It also includes charge distributions and the energetics for the reactant, products, intermediates, and transition states for various reactions involved in dehydrogenation, hydrocarbon oxidation, and metal reoxidation reactions.

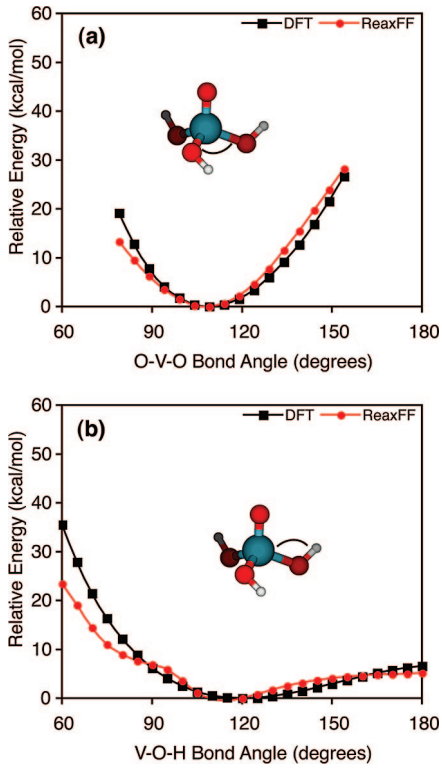

Figure 2. Comparison of ReaxFF and QM valence angle curves for (a) the O−V−O angle and (b) the V−O−H angle in O═V(OH)$_3$.

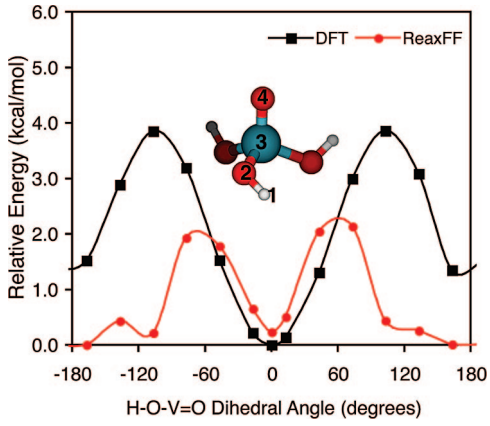

Figure 3. Comparison of the ReaxFF and QM rotational barrier for the V−O bond in O═V(OH)$_3$ to describe the H−O−V^V−O dihedral angle.

This QM-based training set was used to optimize the parameters for the ReaxFF description for vanadium oxides while ensuring that the final parameters retained their quality with regard to the hydrocarbon training set.[16,26]

3.1. Bond Dissociation. DFT calculations were performed to determine the bond dissociation energies for various V═O, V−O, V−H, and V−C bonds. Since the single determinant description used in DFT can lead to a poor description of the singlet state at large separation distances,[40,41] we also performed calculations on the triplet state to define the correct dissociation energies. Thus, the ReaxFF describes the singlet state until near the dissociation limit, where it describes the triplet state.

Figure 1 provides examples of the QM data for bond dissociations and the results obtained from ReaxFF. Figure 1a shows the V═O double bond dissociation in V_4O_{10} clusters, while Figure 1b shows the results for V−OH single bond dissociation in $VO(OH)_3$. The bond dissociation curves for

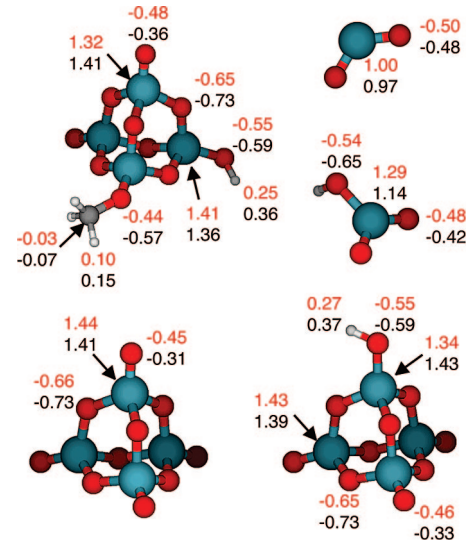

Figure 4. Comparison of the Mulliken charge distributions obtained from DFT (black, bottom number) and charge distributions obtained from ReaxFF (red, top number).

$H_3C-VO(OH)_2$ and $H-VO(OH)_2$ are shown in Figure 1c and d, respectively. In each case, bond parameters were optimized with respect to the lowest-energy points on the dissociation curves, with the most weight given to the equilibrium geometry and dissociation energy.

The calculated adiabatic QM bond energies (kcal/mol) are 118 for V═O, 82 for V−OH, 52 for V−C, and 55 for V−H. Except for V−O where ReaxFF is low by 10 kcal/mol, the ReaxFF bond energies are within 1−3 kcal/mol of the QM results. For all of these systems, ReaxFF provides a good description of the various dissociation energies and equilibrium bond distances. In addition to the bonds shown in Figure 1, the training set also includes the bond dissociation curves for (1) V═O and V−OH bond dissociations in $VO_2(OH)$, (2) the V−O single bond in the overoxidized the $VO_2(OH)_2$ cluster, and (3) the O−O single bond of $O_2V-O-O-VO_2$ to form 2 VO_3.

Our studies of the propane ODH on the V_4O_{10} cluster found a new mechanism, O_2-assisted desorption of water from a V^{III} site, which serves as an essential step in the mechanism for reoxidation of the active site.[8] Therefore, we also included the potential energy surfaces for the O−O bond stretching and the V−O bond stretching in the peroxo group bound to a V_4O_9 cluster. Comparisons between ReaxFF and QM for the additional bond dissociation curves are available in the Supporting Information.

3.2. Valence Angle Terms. The valence angle parameters for ReaxFF were optimized using angle distortion energies obtained from DFT calculations on small vanadium oxide clusters. There are six unique angles relevant to the vanadium oxide/hydrocarbon system including O−V−O, V−O−V, V−O−H, V−O−C, O−V−C, and O−V−H. To cover a variety of bonding environments, nine angle-bending curves obtained from seven unique vanadium oxide clusters were included in the training set. For each case, angle constraints were employed for the internal coordinate of interest, while the remaining degrees of freedom were relaxed during the minimization. Figure 2 shows a comparison between the ReaxFF and DFT energies as a function of valence angle for the O−V−O and V−O−H angles in O═V(OH)$_3$. ReaxFF and DFT results for the remaining seven angles are available in the Supporting Information.

3.3. Dihedral Angle Terms. To optimize the dihedral parameters in ReaxFF, the DFT rotational barriers were

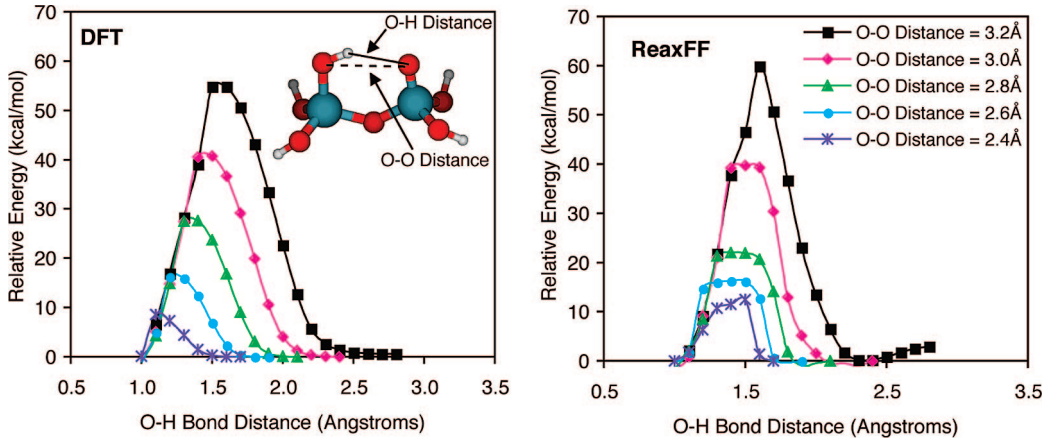

Figure 5. QM and ReaxFF potential energy surfaces for transfer of the hydrogen from the hydroxyl group (V^{IV}−OH) to the vanadyl group (V^{V}=O). The reaction profiles are shown for a range of O−O distances.

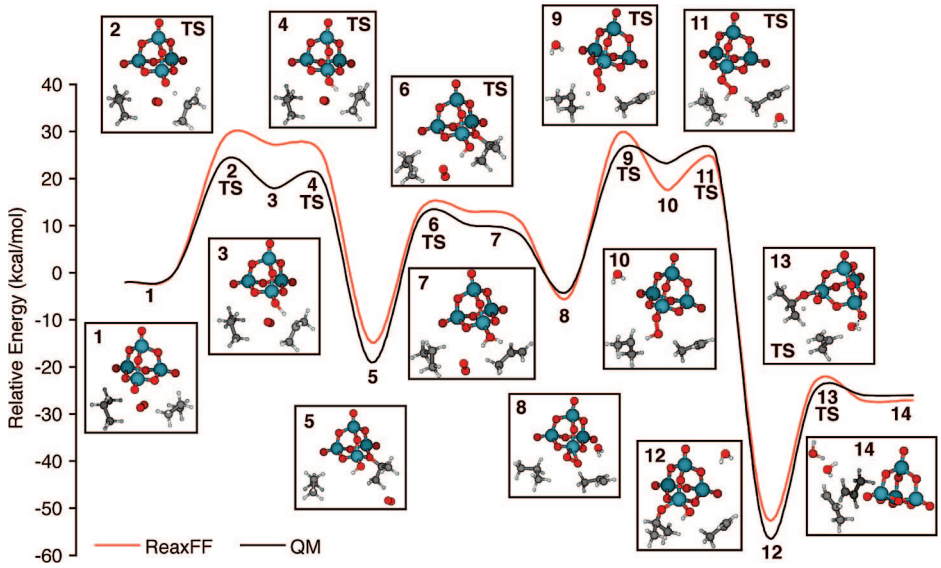

Figure 6. Comparison between the QM and ReaxFF potential energy surfaces for the ODH conversion of two propane molecules on a V_4O_{10} cluster proceeding via the SS-VAFR mechanism.[8] The structures that correspond to transition states have been labeled TS.

calculated by constraining the appropriate dihedral angle while relaxing the rest of the cluster. Six rotational barriers were calculated corresponding to rotation about V−O and C−O bonds to describe C−C−O-V^{IV}, H−C−O-V^{IV}, C−O−V^{V}=O, C−O−V^{IV}−O, H−O−V^{V}=O, and H−O−V^{IV}−O systems. Comparison between the DFT and ReaxFF rotational barriers for the V−O bond in O=V$(OH)_3$ is shown in Figure 3, while the results for the remaining five rotational barriers are included in the training set and are available in the Supporting Information. All of the dihedral angles have small rotational barriers of less than 5 kcal/mol, and ReaxFF is able to reproduce this feature quite well.

3.4. Charge Distributions. ReaxFF uses an energy expression to optimize the charges. This employs electronegativity, hardness, and shielding atomic charge parameters for each element. ReaxFF charge distributions are calculated using the electronegativity equalization method (EEM).[31] The charge parameters are optimized using Mulliken charge distributions obtained from DFT calculations on 20 vanadium oxide clusters. Figure 4 compares the charge distributions from QM and ReaxFF for 5 of these 20 clusters, where we see that ReaxFF successfully reproduces the charge distributions. The comparisons for the remaining 18 molecules included in the training set for parameterization of the ReaxFF force field are in the Supporting Information.

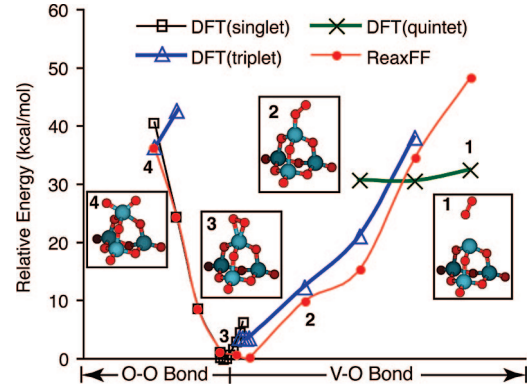

Figure 7. Comparison of potential energy surfaces from QM and ReaxFF for stretching of the V−O bond (**3** → **1**) and O−O bond (**3** → **4**) for the peroxyl group bound to a V_4O_8 cluster, where **3** corresponds to the ground state.

3.5. Reaction Energies. The training set also includes a variety of reaction energies and mechanisms relevant to the ODH chemistry of vanadium oxide catalysts. Migration of

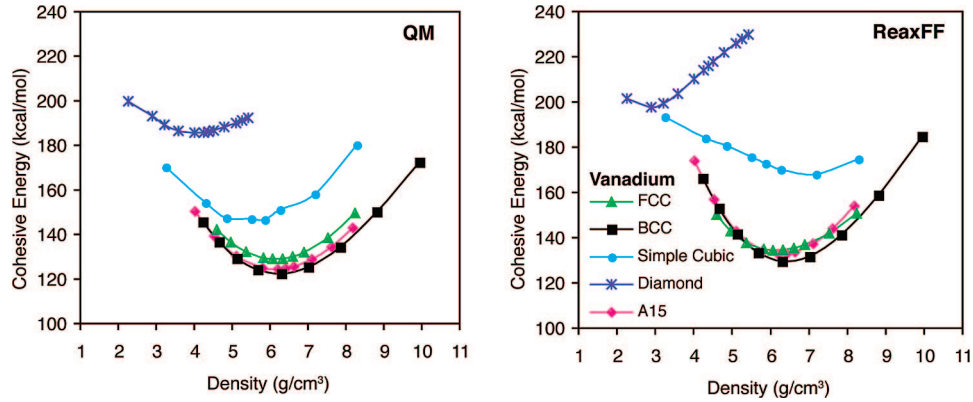

Figure 8. Equation of state (compression/expansion) for five phases of vanadium calculated using periodic DFT and ReaxFF methods.

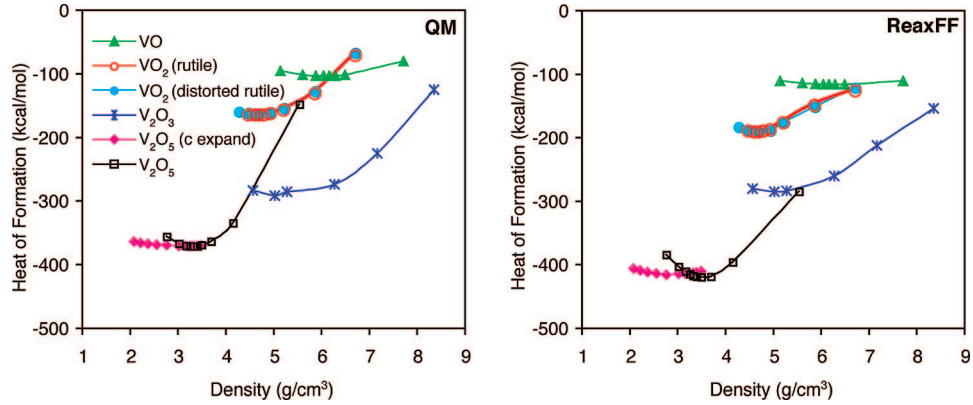

Figure 9. Equation of state (compression/expansion) for phases of vanadium oxide calculated by periodic DFT and ReaxFF methods. The heat of formation for each phase was calculated relative to dioxygen and the ground-state of vanadium, V(bcc).

hydrogen as well as hydrogen transfers resulting in water formation on the vanadium oxide surface are important steps related to regeneration of the catalyst during ODH. We have performed DFT calculations to determine the barrier for migration of hydrogen from a hydoxyl group ($V^{IV}-OH$) to a vanadyl group ($V^{V}=O$) in a model vanadium oxide cluster, and the comparison with ReaxFF barriers is shown in Figure 5. The barrier for hydrogen transfer decreased as the distance between the two oxygens decreased, and ReaxFF was able to correctly reproduce this feature.

We also included in the training set the full pathway for the single-site vanadyl activation, functionalization, and reoxidation (SS-VAFR) mechanism using the V_4O_{10} cluster, which provided key barriers and thermodynamics for the propane ODH processes.[8] Here, each intermediate 1, 3, 5, 7, 8, 10, 12, and 14 was minimized with QM and ReaxFF. For the transition states, the QM results were based on calculating the analytic Hessian and optimizing while retaining a single negative eigenvalue. For ReaxFF, we applied bond restraints to find the lowest-energy pathway from the reactant to the product, where a maximum on this pathway is considered to be transition state. The comparison between the QM and ReaxFF potential energy surfaces in Figure 6 shows that ReaxFF captures the energetics of the various reactions comprising the propane ODH pathways from initiation to catalyst regeneration.

An interesting aspect of the SS-VAFR mechanism is the dioxygen-assisted desorption of water to form a peroxy group on the vanadium oxide cluster (steps 7 and 8), which is then used in subsequent ODH reactions (steps 9 to 14). The energetics for stretching the O−O and V−O bonds in the bound peroxy group in structure **3** (Figure 7) were included in the ReaxFF training set, and the comparison with QM is shown in Figure 7.

The training set also includes QM data for other reactions relevant to ODH on vanadium oxide, including the following:

(1) energetic differences between various small vanadium oxide clusters (e.g., V_2O_4, V_2O_5, V_2O_6, and V_3O_6) reported by Calatayud et al.,[42]

(2) oxidation/reduction of small vanadium oxide clusters (e.g., $V_4O_9 + 1/2\ O_2 \rightarrow V_4O_{10}$, where $E_{QM} = -59.0$ kcal/mol and $E_{ReaxFF} = -56.1$ kcal/mol),

(3) reduction of vanadium oxide clusters with hydrogen and carbon (e.g., $V_4O_{10}\ H \rightarrow V_4O_9(OH)$, where $E_{QM} = -78.1$ kcal/mol and $E_{ReaxFF} = -84.0$ kcal/mol),

(4) strength of V−O single and double bonds in over/undercoordinated vanadium oxide clusters (such as VO_3 and $V(OH)_3$), and

(5) thermodynamics of the conversion of methane to formaldehyde on a V_4O_{10} cluster.

This diversity of the training set as well as the energetics related to vanadium atoms in different coordination environments allows us to optimize the relationship between the bond order, coordination, and valence angles. Comparisons between QM and ReaxFF for these reactions are supplied in the Supporting Information.

3.6. Condensed-Phase Data. A key application for this force field involves the simulation of condensed-phase vanadium oxide systems exposed to hydrocarbons, where the ability of ReaxFF to access various oxidation states during catalysis is crucial for successful simulations. For both vanadium metal and vanadium oxide crystal phases, we performed DFT calculations on periodic cells over a wide volume range to obtain equations

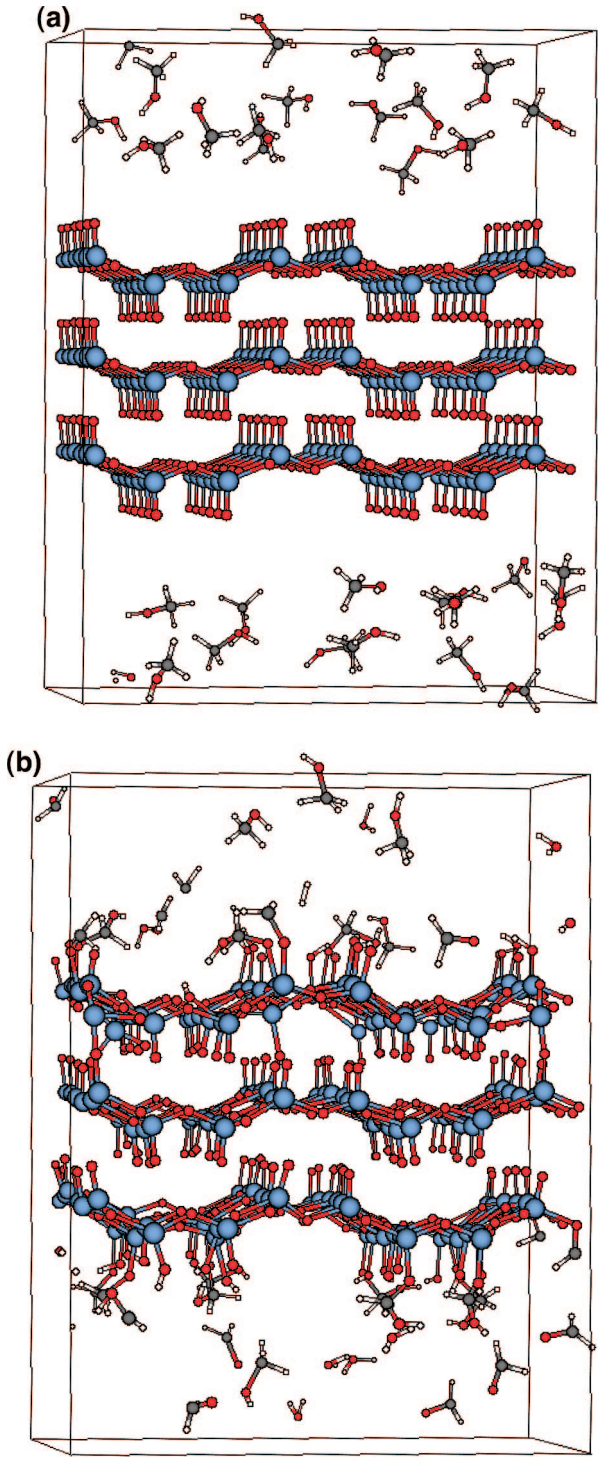

Figure 10. (a) Initial minimized configuration of the CH_3OH/V_2O_5 system. (b) Final configuration after a 250 ps NVT-MD simulation. The periodic system is composed of 30 methanol molecules exposed to the 001 surface of a three-layer V_2O_5 slab.

of state and stabilities of the various phases with different V coordinations.

The most stable form of vanadium crystal is body-centered cubic (bcc), with two atoms per cubic cell and an experimental cohesive energy of 122.46 kcal/mol,[43] which compares quite well with the ReaxFF value of 129.55 kcal/mol. The QM results for the bcc crystal and four other phases [face-centered cubic (fcc), a15, simple cubic (sc), and diamond] are compared with ReaxFF in Figure 8. ReaxFF correctly reproduces the lattice parameters, density, and relative stability of the three most stable

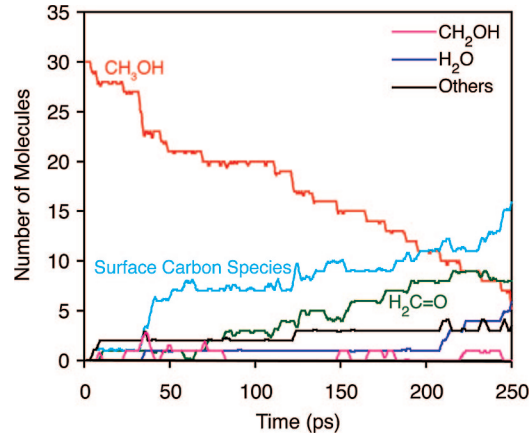

Figure 11. Product distribution observed during the NVT-MD simulation of CH_3OH exposed to $V_2O_5(001)$. Only major products are shown explicitly; minor intermediates are included as "others", and carbon-containing intermediates bound to the V_2O_5 surface are included as "surface carbon species".

metal phases; however, for the sc and diamond phases, ReaxFF reproduces the relative stability but not the density. These low-coordinate sc and diamond crystals are less stable by 40−80 kcal/mol and, hence, are of little importance; they were given low weight during the optimization of the force field.

Since vanadium oxide condensed phases are key components of many heterogeneous catalyst systems, we included in the ReaxFF training set QM data for heats of formation and a range of densities for a variety of vanadium oxide crystal structures. These consist of the VO fcc phase, the V_2O_3 corundum phase, the low-temperature distorted rutile phase of VO_2, the high-temperature symmetric rutile phase of VO_2, and the most stable phase, V_2O_5. This covers the important III, IV, and V oxidation states plus less stable over/underoxidized systems. Here, we included both cubic compression and expansion and compression and expansion in the *c* direction to capture the weak interlayer bonding in the V_2O_5 structure.

Figure 9 compares the results for ReaxFF to QM for the various phases, and ReaxFF provides a good description of the lattice parameters and densities. We find that ReaxFF leads to energy differences for various oxidation changes in good agreement with QM (Figure 9), but ReaxFF tends to underestimate the overall stability of the vanadium oxide phases.

Summarizing, ReaxFF capture the energetics for redox reactions occurring on vanadium oxide surfaces.

3.7. Application to ODH of Methanol on $V_2O_5(001)$. To test the validity of the ReaxFF method for describing the ODH reactions on vanadium oxide catalysts, we performed NVT-MD simulations on a system containing a $V_2O_5(001)$ slab at 650 K exposed to a gas of 30 methanol molecules at 2000 K for 250 ps. The initial configuration of the system is shown in Figure 10a. The dual-temperature regime was employed to ensure that reactions were observed on our time scale while preventing the metal oxide from melting.

First, we carried out a NVT-MD simulation at 2000 K for 1000 ps with just the 30 methanol molecules in a periodic box ($20 \times 20 \times 20$ Å^3, the same as the region available in the CH_3OH/V_2O_5 simulation). No reactions were observed during the simulation time, indicating that under these conditions, methanol does not decompose.

The product distribution from the CH_3OH/V_2O_5 simulation is shown over the full 250 ps in Figure 11. As expected, the first step involves hydrogen abstraction of the methyl hydrogen by a surface vanadyl group (V=O) to form a surface hydroxyl

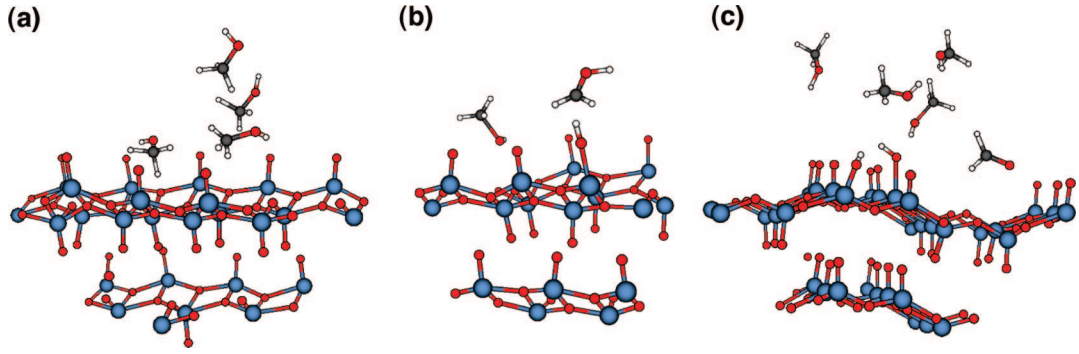

Figure 12. Snapshots from the CH_3OH/V_2O_5 ReaxFF simulation showing the conversion of methanol to formaldehyde. Snapshot (a) obtained at 3.425 ps shows the system prior to the first reaction. Snapshot (b) obtained at 3.45 ps shows the first hydrogen abstraction by a surface V═O to form the CH_2OH radical and a surface hydroxl group. Snapshot (c) obtained at 8.8 ps shows that the second hydrogen abstraction by a surface V═O has resulted in the formaldehyde product and a second surface hydroxyl group. Atoms are shown within 10 Å of the reacting V═O group.

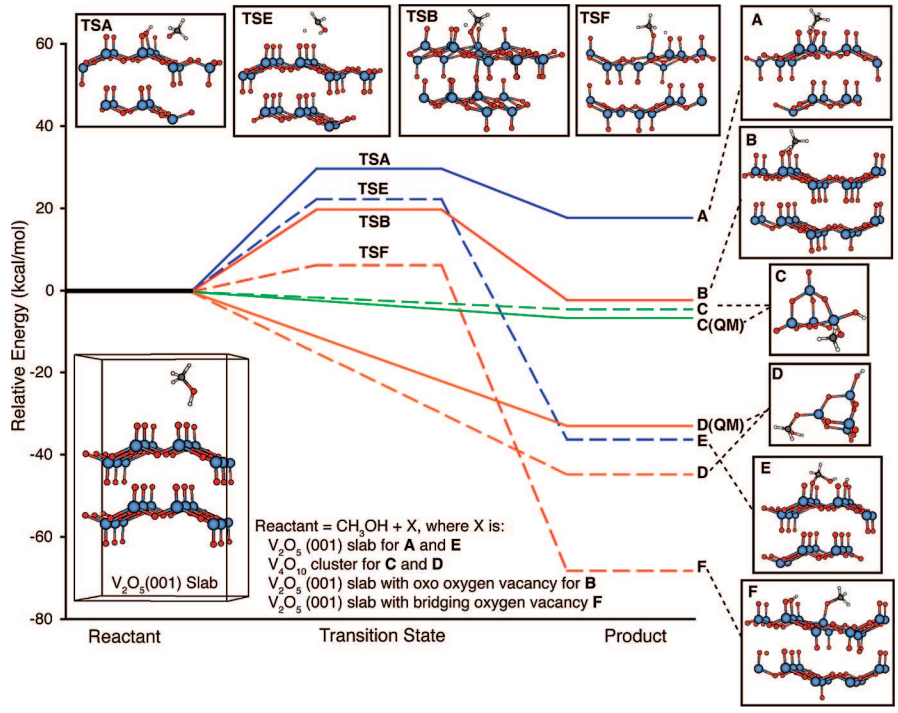

Figure 13. Energetics for the initial hydrogen abstraction from methanol over model vanadium oxide catalysts. The blue lines correspond to using a fully oxidized $V_2O_5(001)$ slab where a surface V═O abstracts a hydrogen from the methyl group (broken line, path A) of methanol to form surface hydroxyl and $-OCH_2OH$ groups or from the hydroxyl group (solid line, path E) of methanol to form surface hydroxyl and methoxy groups. The red lines correspond to using a $V_2O_5(001)$ surface with a defect created by an oxygen vacancy at either an oxo site (solid line, path B) or a bridging oxygen site (broken line, path F). In both cases, coordination of methanol to the reduced vanadium defect site is followed by abstraction of the hydrogen from the hydroxyl group by a neighboring V═O. QM (green, solid line) and ReaxFF (green, broken line) energetics are provided for the O−H dissociation reaction, $V_4O_{10} + CH_3OH \rightarrow V_4O_9(OH)(OCH_3)$, path C. QM (orange, solid line) and ReaxFF (orange, broken line) energetics are provided for the C−H dissociation reaction, $V_4O_{10} + CH_3OH \rightarrow V_4O_8(OH)(OCH_2OH)$, path D.

group and CH_2OH radical (Figure 12b). The CH_2OH radical intermediate is a very short-lived species associated with the surface oxygens, which converts rapidly (5 ps) to formaldehyde (Figure 11). This formaldehyde is formed by a second hydrogen abstraction by a different vanadyl group, yielding a second surface hydroxyl group and the formaldehyde product (Figure 12c), in agreement with experiment.[2,44] Snapshots from the trajectory showing these processes are included in Figure 12. The simulation was continued for an additional 250 ps, and CO_x and H_2 were produced by decomposition of formaldehyde, which is consistent with experiments a higher temperatures.[45,46]

Indeed, in situ DRIFTS study[47] of the adsorption and oxidation of CH_3OH on V_2O_5 suggests that below 548 K, the mechanism proceeds via chemisorption of the methanol on the surface to form surface methoxy and hydroxy groups. This

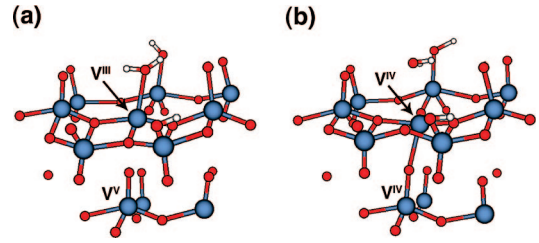

Figure 14. Snapshots from the CH_3OH/V_2O_5 ReaxFF simulation showing the desorption of water. Water formation occurs from hydrogen migration from neighboring hydroxyl groups as in Figure 12c. In (a), a water molecule is coordinated to a V^{III} site with a V^V═O in the second layer. In (b), the dissociation of water results in an interlayer bond forming two V^{IV}. Atoms are shown within 5.5 Å of the vanadium coordinated to the water molecule.

seems to contradict the findings from our molecular dynamics simulations, where we found that the initial hydrogen abstractions occurred exclusively by C−H, rather than O−H, bond dissociation. We believe that this discrepancy might be due to the presence of lower-oxidation defect sites in the experiment, which were absent in our simulations. To investigate this, we performed a number of reaction path scans with ReaxFF, where we studied the dissociation paths on defect and nondefect V_2O_5 slabs. We found, in accordance with our MD results, that on nondefect slabs, the C−H dissociation (path E, Figure 13) is greatly preferred over the O−H dissociation (path A, Figure 13). Once we created a defect by removing an oxo group (path B, Figure 13) or a bridge oxygen (path F, Figure 13), we found that this provides a low-barrier pathway for O−H dissociation, which is initiated by the methanol oxygen binding to the reduced vanadium defect site. These ReaxFF pathways were confirmed by QM simulations on V_4O_{10} clusters, where we found that for the fully oxidized cluster, the C−H dissociation product (path D(QM)) is preferred over the O−H dissociation product (path C(QM)). These findings confirm that, on the fully oxidized slab as used in our simulations, the C−H dissociation path is preferred over the O−H dissociation path. In addition, these results correlate with recent experimental and theoretical results for the V_2O_3 surface,[48,49] which find that oxidation of the V_2O_3 surface leads to formation of vanadyl (V^{+5}═O) groups while the vanadium in the bulk remains V^{+3}. The degree of oxidation of the surface has been shown[49] to be related to the selective conversion of methanol to formaldehyde, where a partially oxidized surface with both V^{+3} and V^{+5}═O is optimal.

In addition to the production of formaldehyde, we observe formation of water during the NVT-MD simulation. The initial step in the production of water is the formation of a water molecule coordinated to a surface V^{III} site. This occurs through transfer of hydrogen from one surface hydroxyl group to another. On the basis of the QM data included in the training set (Figure 5), the barrier for the hydrogen transfer decreases as the distance between neighboring groups decreases. Therefore, vibrational excursion resulting in this distance becoming shorter will facilitate hydrogen mobility on the catalyst surface. Figure 14 shows a reaction sequence from the dynamics, showing such an event.

Once water has formed on the catalyst surface, one might expect it to desorb directly to form a free water molecule. However, Cheng et al.[8] found that the dissociation of water directly from a V^{III} site on a small vanadium oxide cluster is endothermic by 37.8 kcal/mol, which in our ReaxFF simulations is similar, 34.5 kcal/mol. However, Cheng showed that binding dioxygen to the surface reduced this barrier to 12.9 kcal/mol. Periodic DFT calculations by Fu et al.[11] investigating the ODH of propene showed that direct desorption of water from the V_2O_5 surface was endothermic by a similar amount (13.0 kcal/mol) due to the formation of a stabilizing interlayer bond. We do not have dioxygen present in our simulations; therefore, desorption of water from the catalyst surface must occur through another mechanism, perhaps along the lines of the one proposed by Fu et al.[11] Figure 14a shows the configuration of the system with the water coordinated to a V^{III} site, while a V^{V}═O is present in the second layer. In Figure 14b, the water has dissociated simultaneously with formation of an interlayer bond (V^{IV}−O−V^{IV}). Thus, the interlayer bonding stabilizes the surface vanadium site to facilitate desorption of water. This results is not only consistent with Fu's proposed mechanism, but it is also consistent with a temperature-programmed desorption (TPD) study,[50] which found that water desorbed at 390 K. This result is a nice example of ReaxFF allowing realistic simulations that lead to discovering an unexpected reaction mechanism even where it is not parameterized directly for it.

4. Conclusions

In order to enable the study of hydrocarbon oxidation on multimetal oxide catalysts, we developed the ReaxFF reactive force field to describe accurately hydrocarbon reactions with vanadium oxide catalysts. A substantial training set of QM data for a wide variety of structures and energetics relevant to hydrocarbon oxidation and dehydrogenation by vanadium oxide clusters and for reoxidation of these clusters was used to extend the parameterization of the ReaxFF force field to include these reactions. We validated that the ReaxFF force field provides a good description of the QM data training set including the energy differences for oxidation state changes of vanadium in condensed-phase systems. This indicates that ReaxFF is capable of capturing the energetics of redox reactions for vanadium oxides.

To demonstrate the capability of the ReaxFF force field, we carried out ReaxFF-MD simulations on a system containing 30 methanol molecules exposed to a V_2O_5(001) slab. We observed the conversion of methanol to formaldehyde, in agreement with experiment. The mechanism involves hydrogen abstraction of the methyl hydrogen by a surface vanadyl (V═O) group to form a CH_2OH radical and a surface hydroxy group followed by a subsequent hydrogen abstraction by another V═O group to form an additional surface hydroxy group and the formaldehyde product. In addition, we observed desorption of water, in agreement with TPD experiments. The desorption from a V^{III} site was found to be facilitated by interlayer bonding to the vanadyl oxygen of a second-layer V^{V} site, resulting in converting V^{V}═O···V^{III}···OH_2 to two V^{IV} sites [V^{IV}−O−V^{IV}] and a water molecule.

Thus, the results from the NVT-MD simulation are in good agreement with experimental observations, indicating that ReaxFF provides a useful tool for studying the reactions of hydrocarbons on vanadium oxide surfaces.

Acknowledgment. This research was supported, in part, by funds from NSF (ITR-DMR-0427177) and ONR (N00014-05-1-0778)

Note Added after ASAP Publication. This article was posted ASAP on July 25, 2008 in *The Journal of Physical Chemistry A*. After ASAP, the paper was reassigned to *The Journal of Physical Chemistry C*. The corrected version was posted on August 19, 2008.

Supporting Information Available: Description of the full ReaxFF potential functions, force field parameters described in this manuscript, and figures showing comparison between ReaxFF and QM energies for training set. This material is available free of charge via the Internet at http://pubs.acs.org.

References and Notes

(1) Tatibouet, J. M.; Germain, J. E. *CR Acad. Sci. II C* **1979**, *298*, 305.

(2) Forzatti, P.; Tronconi, E.; Elmi, A. S.; Busca, G. *Appl. Catal., A* **1997**, *157*, 387.

(3) (a) Ushikubo, T.; Nakamura, H.; Koyasu, Y.; Wajiki, S. U.S. Patent 5380933, January 10, 1995. (b) Ushikubo, T.; Oshima, K.; Ihara, T.; Amatsu, H. U.S. Patent 5534650, July 8, 1996.

(4) DeSanto, P., Jr.; Buttrey, D. J.; Grasselli, R. K.; Lugmair, C. G.; Volpe, A. F., Jr.; Toby, B. H.; Vogt, T. *Z. Kristallogr.* **2004**, *219*, 152.

(5) Grasselli, R. K. *Catal. Today* **2005**, *99*, 23.

(6) Holmberg, J.; Haggblad, R.; Andersson, A. *J. Catal.* **2006**, *243*, 350.
(7) Pudar, S.; Oxgaard, J.; van Duin, A. C. T.; Chenoweth, K.; Goddard, W. A., III. *J. Phys. Chem. C* **2007**, *111*, 16405.
(8) Cheng, M.-J.; Chenoweth, K.; Oxgaard, J.; van Duin, A. C. T.; Goddard, W. A., III. *J. Phys. Chem. C* **2007**, *111*, 5115.
(9) Argyle, M. D.; Chen, K. D.; Bell, A. T.; Iglesia, E. J. *Phys. Chem. B* **2002**, *106*, 5421.
(10) Argyle, M. D.; Chen, K. D.; Bell, A. T.; Iglesia, E. *J. Catal.* **2002**, *208*, 139.
(11) Fu, H.; Liu, Z.-P.; Li, Z.-H.; Wang, W.-N.; Fan, K.-N. *J. Am. Chem. Soc.* **2006**, *128*, 11114.
(12) Rozanska, X.; Fortrie, R.; Sauer, J. *J. Phys. Chem. C* **2007**, *111*, 6041.
(13) Boulet, P.; Baiker, A.; Chermette, H.; Gilardoni, G.; Volta, J.-C.; Weber, J. *J. Phys. Chem. B* **2002**, *106*, 9659.
(14) Dobler, J.; Pritzsche, M.; Sauer, J. *J. Am. Chem. Soc.* **2005**, *127*, 10861.
(15) Goodrow, A.; Bell, A. T. *J. Phys. Chem. C* **2007**, *111*, 14753.
(16) Chenoweth, K.; van Duin, A. C. T.; Goddard, W. A., III. *J. Phys. Chem. A* **2008**, *112*, 1040.
(17) Strachan, A.; Kober, E.; van Duin, A. C. T.; Oxgaard, J.; Goddard, W. A., III. *J. Chem. Phys.* **2005**, *122*, 054502.
(18) Strachan, A.; van Duin, A. C. T.; Chakraborty, D.; Dasgupta, S.; Goddard, W. A., III. *Phys. Rev. Lett.* **2003**, *91*, 098301.
(19) van Duin, A. C. T.; Seiri, Y.; Dubnilova, F.; Kosloff, R.; Goddard, W. A., III. *J. Am. Chem. Soc.* **2005**, *127*, 11053.
(20) Chenoweth, K.; Cheung, S.; van Duin, A. C. T.; Goddard, W. A., III; Kober, E. M. *J. Am. Chem. Soc.* **2005**, *127*, 7192.
(21) Goddard, W. A., III; Merinov, B.; van Duin, A. C. T.; Jacob, T.; Blanco, M.; Molinero, V.; Jang, S. S.; Jang, Y. H. *Mol. Simul.* **2006**, *32*, 251.
(22) Nielson, K. D.; van Duin, A. C. T.; Oxgaard, J.; Deng, W.; Goddard, W. A., III. *J. Phys. Chem. A* **2005**, *109*, 493.
(23) Ludwig, J.; Vlachos, D. G.; van Duin, A. C. T.; Goddard, W. A., III. *J. Phys. Chem. B* **2006**, *110*, 4274.
(24) Goddard, W. A., III.; van Duin, A.; Chenoweth, K.; Cheng, M.-J.; Pudar, S.; Oxgaard, J.; Merinov, B.; Jang, Y. H.; Persson, P. *Top. Catal.* **2006**, *38*, 93.
(25) Chenoweth, K.; Pudar, S.; van Duin, A. C. T.; Cheng, M.-J. *Top. Catal.* . accepted.
(26) van Duin, A. C. T.; Dasgupta, S.; Lorant, F.; Goddard, W. A., III. *J. Phys. Chem. A* **2001**, *105*, 9396.
(27) Pauling, L. *The Nature of the Chemical Bond*, 3rd ed.; Cornell University Press: Ithaca, NY, 1960.
(28) Johnston, H. S.; Parr, C. *J. Am. Chem. Soc.* **1963**, *85*, 2544.
(29) Tersoff, J. *Phys. Rev. B* **1988**, *38*, 9902.
(30) Brenner, D. W. *Phys. Rev. B* **1990**, *42*, 9458.
(31) Mortier, W. J.; Ghosh, S. K.; Shankar, S. J. *J. Am. Chem. Soc.* **1998**, *120*, 261.
(32) van Duin, A. C. T.; Baas, J. M. A.; van de Graaf, B. *J. Chem. Soc., Faraday Trans.* **1994**, *90*, 2881.
(33) (a) Becke, A. D. *J. Chem. Phys.* **1993**, *98*, 5648. (b) Lee, C.; Yang, W.; Parr, R. G. *Phys. Rev. B* **1998**, *37*, 785.
(34) *Jaguar 7.0*; Schrodinger Inc.: Portland, OR, 2007.
(35) Keith, J. A.; Gonzales, J.; Oxgaard, J.; Goddard, W. A., III. Manuscript in preparation.
(36) (a) Hariharan, P. C.; Pople, J. A. *Chem. Phys. Lett.* **1972**, *16*, 217. (b) Francl, M. M.; Pietro, W. J.; Hehre, W. J.; Binkley, J. S.; Gordon, M. S.; DeFrees, D. J.; Pople, J. A. *J. Chem. Phys.* **1982**, *77*, 3654.
(37) (a) Hay, P. J.; Wadt, W. R. *J. Chem. Phys.* **1985**, *82*, 299. (b) Goddard, W. A., III. *Phys. Rev.* **1968**, *174*, 659. (c) Melius, C. F.; Olafson, B. O.; Goddard, W. A., III. *Chem. Phys. Lett.* **1974**, *28*, 457.
(38) Verdozzi, C.; Schultz, P. A.; Wu, R.; Edwards, A. H.; Kioussis, N. *Phys. Rev. B* **2002**, *66*, 125408.
(39) Berendsen, H. J. C.; Postma, J. P. M.; van Gunsteren, W. F.; DiNola, A.; Haak, J. R. *J. Chem. Phys.* **1984**, *81*, 3684.
(40) Fuchs, M.; Niquet, Y.-M.; Gonze, X.; Burke, K. *J. Chem. Phys.* **2005**, *122*, 094116.
(41) Gritsenko, O. V.; Schipper, P. R. T.; Baerends, E. J. *J. Chem. Phys.* **1997**, *107*, 5007.
(42) Catalayud, M.; Andres, J.; Beltran, A. *J. Phys. Chem. A* **2001**, *105*, 9760.
(43) Kittel, C. *Introduction to Solid State Physics*; Wiley: New York, 1976.
(44) Gambaro, L. A. *J. Mol. Catal. A: Chem.* **2004**, *214*, 287.
(45) Burcham, L. J.; Badlani, M.; Wachs, I. E. *J. Catal.* **2001**, *203*, 104.
(46) Bronkema, J. L.; Bell, A. T. *J. Phys. Chem. C* **2007**, *111*, 420.
(47) Sambeth, J E.; Centeno, M. A.; Paul, A.; Briand, L. E.; Thomas, H. J.; Odriozola, J. A. *J. Mol. Catal. A: Chem.* **2000**, *161*, 89.
(48) (a) Guimond, S.; Abu Haija, M.; Kaya, S.; Lu, J.; Weissenrieder, J.; Shaikhutdinov, Sh. K.; Kuhlenbeck, H.; Freund, H.-J.; Döbler, J.; Sauer, J. *Top. Catal.* **2006**, *38*, 117. (b) Kolczewski, C.; Hermann, K.; Guimond, S.; Kuhlenbeck, H.; Freund, H.-J. *Surf. Sci.* **2007**, *601*, 5394.
(49) (a) Freund, H.-J. *Top. Catal.* **2008**, *48*, 137. (b) Romanyshyn, Y.; Guimond, S.; Kuhlenbeck, H.; Kaya, S.; Blum, R. P.; Niehus, H.; Shaikhutdinov, S.; Simic-Milosevic, V.; Nilius, N.; Freund, H.-J.; Ganduglia-Pirovano, M. V.; Fortrie, R.; Döbler, J.; Sauer, J. *Top. Catal.* Accepted.
(50) Moshfegh, A. Z.; Ignatiev, A. *Surf. Sci. Lett.* **1992**, *275*, L650.

JP802134X